HHS Public Access

Author manuscript

ACS Biomater Sci Eng. Author manuscript; available in PMC 2024 May 22.

Published in final edited form as:

ACS Biomater Sci Eng. 2018 July 09; 4(7): 2528–2540. doi:10.1021/acsbiomaterials.8b00408.

Engineering Adhesive and Antimicrobial Hyaluronic Acid/ Elastin-like Polypeptide Hybrid Hydrogels for Tissue Engineering Applications

Ehsan Shirzaei Sani[†], **Roberto Portillo-Lara**[†,‡], **Andrew Spencer**[†], **Wendy Yu**[†], **Benjamin M. Geilich**[†], **Iman Noshadi**[†], **Thomas J. Webster**[†,§], **Nasim Annabi**[*,†,∥,⊥,¥]

[†]Department of Chemical Engineering, Northeastern University, Boston, Massachusetts 02115, United States

[‡]Centro de Biotecnología FEMSA, Tecnológico de Monterrey, Monterrey, Nuevo Leon 64700, México

[§]Wenzhou Institute of Biomaterials and Engineering, Wenzhou Medical University, Wenzhou, China

[∥]Biomaterials Innovation Center, Brigham and Women's Hospital, Harvard Medical School Boston, Massachusetts 02139, United States

[⊥]Harvard-MIT Division of Health Sciences and Technology, Massachusetts Institute of Technology, Cambridge, Massachusetts 02139, United States

Abstract

Hydrogel-based biomaterials have been widely used for tissue engineering applications because of their high water content, swellability, and permeability, which facilitate transport and diffusion of essential nutrients, oxygen, and waste across the scaffold. These characteristics make hydrogels suitable for encapsulating cells and creating a cell supportive environment that promotes tissue regeneration when implanted in vivo. This is particularly important in the context of tissues whose intrinsic regenerative capacity is limited, such as cartilage. However, the clinical translation of hydrogels has been limited by their poor mechanical performance, low adhesive strength, uncontrolled degradation rates, and their susceptibility to bacterial colonization. Here, we introduce an elastic, antimicrobial, and adhesive hydrogel comprised of methacrylated hyaluronic acid (MeHA) and an elastin-like polypeptide (ELP), which can be rapidly photo-cross-linked in situ for the regeneration and repair of different tissues. Hybrid hydrogels with a wide range of physical properties were engineered by varying the concentrations of MeHA and ELP. In addition, standard adhesion tests demonstrated that the MeHA/ELP hydrogels exhibited higher adhesive strength to the tissue than commercially available tissue adhesives. MeHA/ELP hydrogels were

[*]**Corresponding Author**: Nasim Annabi, n.annabi@neu.edu.

[¥]**Present Address:** N.A.: Department of Chemical and Biomolecular Engineering, University of California-Los Angeles, Los Angeles, CA, USA.

ASSOCIATED CONTENT

Supporting Information

The Supporting Information is available free of charge on the ACS Publications website at DOI: 10.1021/acsbiomaterials.8b00408.

Figures S1–S4 (PDF)

The authors declare no competing financial interest.

then rendered antimicrobial through the incorporation of zinc oxide (ZnO) nanoparticles, and were shown to significantly inhibit the growth of methicillin-resistant *Staphylococcus aureus* (MRSA), as compared to controls. Furthermore, the composite adhesive hydrogels supported in vitro mammalian cellular growth, spreading, and proliferation. In addition, in vivo subcutaneous implantation demonstrated that MeHA/ELP hydrogels did not elicit any significant inflammatory response, and could be efficiently biodegraded while promoting the integration of new autologous tissue. In summary, we demonstrated for the first time that MeHA/ELP-ZnO hydrogel can be used as an adhesive and antimicrobial biomaterial for tissue engineering applications, because of its highly tunable physical characteristics, as well as remarkable adhesive and antimicrobial properties.

Graphical Abstract

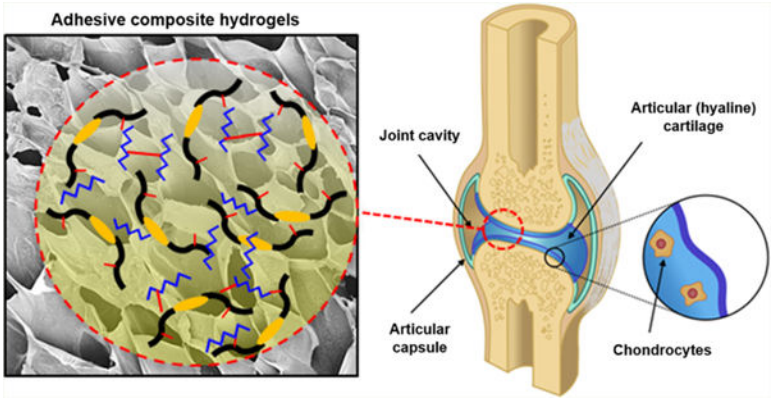

Keywords

tissue engineering; hyaluronic acid; elastin-like polypeptide; antimicrobial hydrogels; adhesive hydrogels

1. INTRODUCTION

Hydrogels are three-dimensional (3D) networks of polymers with high water content and high permeability for the diffusion of essential nutrients and oxygen.[1] As hydrogels mimic the composition and structural properties of the native extracellular matrix (ECM), they possess remarkable potential to be used as scaffolds for regenerative medicine and tissue engineering applications.[2] Hydrogel-based scaffolds should not only have high regenerative capacity and biocompatibility; they should also possess adequate mechanical properties similar to the physiological tissues.[3] In addition, hydrogels intended for tissue repair should be able to adhere to the native tissues and maintain their mechanical stability in the defect site sufficiently long enough to enable regeneration of the damaged tissues.[4] Furthermore, the delivery of progenitor or terminally differentiated cells in combination with regenerative hydrogels could potentially accelerate biointegration and tissue repair at the site of injury.[5] This is particularly important in the context of tissues whose intrinsic regenerative capacity is limited, such as cartilage. In addition, microbial infection is still one of the most severe postoperative complications in clinical orthopedics, which can be

treated by combining antimicrobial agents with hydrogels.[6] Hydrogel-based biomaterials used for cartilage tissue engineering often fail to integrate multiple therapeutic strategies into a single comprehensive approach to enhance the clinical efficacy of tissue engineered scaffolds.[7] Therefore, multifunctional biomaterials with optimal mechanical, adhesive, and antimicrobial properties would constitute a more effective therapeutic strategy over conventional single-strategy approaches for cartilage repair.

Various hydrogel-based biomaterials have been widely investigated in the context of cartilage tissue engineering, due to their ability to be used for 3D cell encapsulation, as well as their ease of modification, high water content, injectability, and biocompatibility.[8] For instance, different types of naturally derived or synthetic-based hydrogels, such as chitosan,[9,10] HA,[11–14] polyethylene glycol (PEG),[15] silk,[16–18] collagen,[19,20] alginate,[21,22] and recombinant elastin-like polypeptides (ELPs),[23] have been used to induce cartilage tissue regeneration and repair.[11,24,25] Among the different biomaterials explored for cartilage repair, HA and ELPs have been shown to possess intrinsic properties that promote the regeneration of cartilage tissue.[26–28] ELPs are stimuli-responsive artificial biopolymers, whose macromolecular structure can be precisely tailored through recombinant DNA techniques.[29] ELPs are derived from elastin, a highly elastic protein that is key for the proper function of cartilage tissue, owing to its role in resisting compressive loads and absorbing the mechanical forces acting on articular joints. Different types of ELPs have been investigated for cartilage tissue engineering, due to their tunable mechanical properties, high elasticity, and ability to promote chondrogenic differentiation.[28,30] However, the engineering of ELP-based hydrogels with controllable physical properties that can be rapidly cross-linked in situ remains technically challenging.[31] On the other hand, HA is a linear, high molecular weight, and nonsulfated glycosaminoglycan (GAG), which is one of the main components of the ECM found in connective tissues.[32] HA is involved in many physiological processes such as cell proliferation, migration, and tissue morphogenesis, as well as new tissue formation.[11] It has been widely reported that HA promotes chondrogenesis by interacting with specific cell surface receptors such as CD44 and the hyaluronan-mediated motility receptor (RHAMM).[32–36] However, previous studies have reported that HA-based hydrogels undergo rapid biodegradation in vivo[37] and lack adequate mechanical stability due to the high hydrophilicity and thus swelling capacity of HA.[38] Furthermore, hydrogels with increasing concentrations of HA often exhibit high mechanical stiffness and reduced elasticity and resilience, which may limit their potential application for cartilage tissue repair.[39,40] Therefore, previous groups have investigated the engineering of hybrid hydrogels based on the combination of both HA and ELPs.[23,41] However, these approaches were hindered by complex and time-consuming chemistries, as well as uncontrollable and slow cross-linking rates. Difficulties such as this may limit the translation of the biomaterials to a clinical setting, since it might not be practical to administer the hydrogel as a standalone material during surgery. Efforts to impart polymers like these with faster and more controlled cross-linking chemistry with minimal processing requirements, while maintaining their regenerative capacity, could significantly expedite their translation to a clinical setting.

In addition to mechanical properties, the adhesive properties of hydrogels can be finely tuned to enhance the adherence of the biomaterial to the target tissue, and support

tissue regeneration under physiological mechanical loads.[42] For instance, Wang et al. demonstrated the advantages of applying a primer layer to cartilage to enhance the adhesive strength of the biomaterial at the material-tissue interface.[5] However, the cells encapsulated in the implanted material were primary chondrocytes from another animal, which may limit its translation into the clinical setting. In another study, Balakrishnan et al. developed an adhesive alginate/gelatin based hydrogel for cartilage tissue regeneration.[21] The engineered hydrogel could integrate well with the host cartilage and facilitate migration and differentiation of chondrocytes. However, further improvement is required to use this adhesive hydrogel for treatment and management of the early stage of osteoarthritis, where defects are small and often associated with a poor healing mechanism.[21] Although the engineered hydrogels showed promising characteristics as biomaterials for cartilage tissue regeneration, the incorporation of antimicrobial agents in their structure can further improve their potential applications for cartilage repair in the actual clinical setting, which are generally affected by microbial infections.

Microbial infections are still associated with severe postoperative complications in orthopedic surgeries, due to the low vascularization of cartilage and host protein adsorption to implanted biomaterials in vivo, which presents a hydrated substrate for microbial colonization.[38] Thus, the incorporation of antimicrobial agents into biomaterials, such as antibiotics, antimicrobial peptides, and metal nanoparticles have been investigated for the prevention of bacterial infection, biofilm formation, and rejection of biomedical implants.[43] The use of metal oxide nanoparticles as antimicrobial materials is one of the most promising strategies for overcoming bacterial infections. In this regard, zinc oxide (ZnO) nanoparticles have been shown to elicit antimicrobial activity against antibiotic-resistant bacteria, through the disruption of bacterial cell membranes and the induction of reactive oxygen species production.[43] Various types of antimicrobial biomaterials have been developed for cartilage tissue repair through incorporation of ZnO nanoparticles in the hydrogel networks; however, most of these biomaterials suffered from low adhesion to the native tissue or lack of biocompatibility.[44,45] Therefore, there is an unmet need to engineer multifunctional antimicrobial hydrogels with tunable biodegradation rates, adequate mechanical properties, and adhesive strength for promoting cartilage tissue regeneration and repair.

Here, we describe the engineering of a new class of hybrid hydrogel adhesives for tissue engineering applications, based on the free radical photopolymerization of methacrylated HA (MeHA) and a custom ELP with photopolymerizable cysteine groups. Next, we investigated the tissue adhesion properties of ELP-based composite hydrogels, following American Society for Testing and Materials (ASTM) standard tests, such as lap shear adhesion and burst pressure resistance. In addition, we incorporated ZnO nanoparticles into the engineered hydrogels to impart them with antimicrobial activity. Liquid MeHA/ELP precursors can be readily delivered to the injury site and be rapidly photo-cross-linked in situ in a safe and controllable manner. Chemical, physical, and biological characterizations of MeHA/ELP hydrogels, including compressive and tensile modulus/strength, water uptake capacity, porosity, in vitro antimicrobial activity, and well as in vitro and in vivo biocompatibility were conducted. Our results suggest that MeHA/ELP-ZnO hydrogels hold remarkable potential for tissue engineering application especially cartilage repair, because of

their highly tunable physical properties, as well as their intrinsic antimicrobial and adhesive properties.

2. MATERIALS AND METHODS

2.1. Synthesis of Methacrylated Hyaluronic Acid (MeHA).

Methacrylated HA (MeHA, molecular weight, 1.6×10^6 Da) was synthesized as described elsewhere.[46] Briefly, methacrylic anhydride (MA) was added to a solution of 1%(w/v) HA in deionized water (DW) and reacted on ice (4 °C) for 24 h. During the reaction, the pH was adjusted to 8 using 5 N NaOH. The solution was then purified using dialysis tubes (MW cutoff 6–8 kDa) against DW for 48 h. Lastly, the product was lyophilized and stored at −20 °C.[47]

2.2. Synthesis and Expression of Elastin-like Polypeptide (ELP).

The photo-cross-linkable ELP sequence was expressed as described in our previous study.[31] This ELP sequence consisted of 70 repeats of the pentapeptide VPGVG, in which the first valine was replaced with an isoleucine every five pentapeptides (i.e., $([VPGVG]_4[IPGVG])_{14}$). In addition, Lys-Cys-Thr-Ser (KCTS) residues were added to both sides of the ELP sequence to render it photo-cross-linkable. *Escherichia coli* (*E. coli*) was used as a host to express the protein. The purification of the ELP was performed using inverse transition cycling as described elsewhere.[48] Oxidation of cysteine residues in the ELP sequence was avoided by dissolving the ELP in a buffer containing 14.3 mM β-mercaptoethanol, which cleaves disulfide bonds that can form between cysteine residues in proteins, for all steps of the cycling process. The purified ELP solution was then dialyzed in a water bath at 4 °C, and stored at room temperature after lyophilization.

2.3. Fabrication of MeHA/ELP Hybrid Hydrogels.

To form MeHA/ELP hybrid hydrogels, different concentrations of MeHA (1 and 2% (w/v)) and ELP (0, 5, 10 and 15% (w/v)) were mixed in a 0.5% (w/v) solution of Irgacure 2959 as a photoinitiator in deionized water at 4 °C. The precursor solutions were then placed in either tensile (12 mm length, 6 mm width, 1.5 mm height) or compression molds (8 mm diameter, 2 mm height) made of polydimethylsiloxane (PDMS), and photo-cross-linked using UV light (6.9 mW/cm^2, EXFO OmniCure S2000) for 120 s. MeHA/ELP-ZnO hydrogels were prepared by directly adding different concentrations of 20 nm ZnO nanoparticles (0.1% and 0.2% (w/v)) (mkNANO) to the MeHA/ELP precursor solution containing 2% MeHA and 10% ELP. The mixture was gently mixed and photo-cross-linked as described before.

2.4. Characterization of Phase Transition Temperature of MeHA/ELP Prepolymers Using Dynamic Viscosity.

In order to determine phase transition temperature of ELP and MeHA/ELP prepolymer solutions, the dynamic viscosity of the solutions was obtained by rheology test. A rheometer (Discovery Hybrid, TA Instruments, New Castle, DE) equipped with a sand-blasted flat plate with a gap size of 1000 μm and a diameter of 40 mm was used to evaluate the viscosity of the solutions. ELP prepolymer solution (10% w/v) as control and MeHA/ELP solution (2% MeHA and 10% ELP) were prepared in 1× Dulbecco's phosphate-buffered saline (DPBS)

and were then pipetted onto the rheometer, and viscosity was determined as a function of temperature under a constant shear rate of 1 Hz. Temperature was varied at a rate of 2 °C/min from 5 to 40 °C.

2.5. Mechanical Characterization of MeHA/ELP Hydrogels.

MeHA/ELP hydrogels with and without ZnO were prepared using compression or tensile molds as described before and incubated for 2 h in DPBS. The dimensions of the hydrogels were then measured using a caliper. An Instron 5943 mechanical tester was used to perform tensile and cyclic compression tests. For the tensile test, hydrogels were placed between two pieces of double sided tape within tension grips and extended at 1 mm/min until failure. The tensile strain (mm) and load (N) were measured using the Bluehill 3 software. Elastic modulus of the engineered hydrogels was calculated from the slope of the stress–strain curves. For the compression tests, hydrogels were loaded between compression plates in a DPBS water bath. Cyclic compression tests were performed at 70% strain level and a rate of 1 mm/min by performing 8 cycles of loading and unloading. The compressive strain (mm) and load (N) were measured using the Bluehill 3 software. The compressive modulus was determined by obtaining the slope of the linear region (0.05–015 mm/mm strain) of the loading stress (kPa) versus strain (mm/mm) curve. Energy loss was calculated by obtaining the area between the loading and unloading curve for cycle 8 ($n = 4$).

2.6. In Vitro Adhesion Tests.

In Vitro Burst Pressure Test.—Burst pressure of MeHA/ELP adhesive hydrogels with and without ZnO containing different concentrations of MeHA and ELP as well as Evicel (Ethicon, Somerville, NJ, USA) and Coseal (Baxter, Deerfield, IL, USA) were obtained by using a ASTM standard (F2392–04) test as described previously.[3] Porcine intestine was placed between two stainless steel annuli, from a burst pressure apparatus in which the upper piece had a 10 mm diameter hole in its center. A 2 mm diameter defect was created by a 18 gauge syringe needle in the center of porcine intestine. A 30 μL of precursor solution was pipetted onto the defect on the intestine and photo-cross-linked by UV light. The sealed intestine was then placed into the burst pressure testing apparatus, and the burst pressure was directly recorded by a connected to a wireless sensor (Pasco)/PC. For each experiment, at least 3 samples were tested.

In Vitro Lap Shear Test.—Shear resistance of MeHA/ELP adhesive hydrogels containing different concentrations of MeHA, ELP with and without ZnO, as well as two commercially available adhesives, Evicel and Coseal was determined based on a modified ASTM standard (F2255–05) for lap shear strength of tissue adhesive materials. As the substrate, two pieces of glass slides (10 mm × 25 mm) were coated with gelatin solution and was dried at room temperature. A 10 μL prepolymer solution was then photo-cross-linked between two pieces of glass slides. The shear strengths of the samples were then tested using an Instron mechanical tester (5943) by tensile loading with a strain rate of 1 mm/min. The shear strength of the materials was calculated at the point of detaching. For each experiment, at least 3 samples were tested.

2.7. In Vitro Swellability of MeHA/ELP Hydrogels.

MeHA/ELP hydrogels with varying ELP and MeHA concentrations were prepared and lyophilized as described before. Once the dried weights of the hydrogels were recorded, the samples were then immersed in DPBS for 24 h. The swollen gels were removed at different time points from the buffer solution and weighed. The swelling ratio was calculated using eq 1, where SR is swelling ratio, W_s is swollen weight of the hydrogel, and W_0 is the initial dried weight before swelling ($n = 4$):

$$\mathrm{SR} = \frac{W_s - W_0}{W_0} \quad (1)$$

2.8. In Vitro Cell Studies.

2.8.1. Cell Lines.—NIH 3T3 cells (ATCC) were cultured at 37 °C and 5% CO_2 in Dulbecco's Modified Eagle Medium (DMEM) media (Gibco), containing 10% (v/v) fetal bovine serum (FBS) and 1% (v/v) penicillin/streptomycin (Gibco). Human mesenchymal stem cells (hMSCs) (Lonza) were cultured at 37 °C and 5% CO_2 in complete mesenchymal stem cell growth medium (MSCGM, Lonza). Cells were maintained in tissue culture treated polystyrene flasks and passaged 1:6 at 70% confluency. hMSC of passage 3–5 were used for all studies.

2.8.2. 2D Cell Seeding on Engineered Hydrogels.—MeHA/ELP hydrogels with 2% MeHA and 10% ELP concentrations with and without ZnO (0.2%(w/v)) were used for 2D culture studies. Hydrogels were formed by pipetting 7 μL of MeHA/ELP precursor solution between a 3-(trimethoxysilyl) propyl methacrylate (TMSPMA, Sigma-Aldrich) coated glass slide and a glass coverslip separated with a 300 μm spacer. Hydrogels were photo-cross-linked upon UV light exposure (6.9 mW cm^{-2} UV light (365 nm)). The hydrogels were then seeded with hMSCs (2×10^6 cells/mL) and NIH 3T3 cells (5×10^6 cells/mL) and maintained at 37 °C and 5% CO_2 for 5 days.

2.8.3. Cell Proliferation.—Cell proliferation was evaluated using a commercial PrestoBlue assay (Fisher) on days 0, 1, 3, and 5 according to instructions from the manufacturer. Briefly, 40 μL of PrestoBlue dye (10% of medium volume) was added to 360 μL of medium (total volume = 400 μL). Cell seeded scaffolds were incubated in the PrestoBlue/medium solution for 45 min at 37 °C. The fluorescence intensity of the resulting solutions was recorded at 535–560 nm excitation and 590–615 nm emission wavelength at different culture times on days 1, 3, and 5. The relative fluorescence intensity of negative controls was recorded using a hydrogel without cells, culture medium, and PrestoBlue dye, and subtracted from all the samples to account for the background ($n = 4$).

2.8.4. Cell Viability.—A commercial calcein AM/ethidium homodimer-1 live/dead assay (Invitrogen) was used to evaluate cell viability according to instructions from the manufacturer. Cell viability was evaluated after 1 h (day 0), and then after 1, 3, and 5 days of culture. Briefly, culture medium was removed from the wells containing cell-seeded hydrogels and the samples were then incubated with 0.5 μL/mL of calcein AM and 2 μL/mL

of ethidium homodimer in DPBS for 15 min in the dark at 37 °C. Live cells were stained green, whereas dead cells were stained red. The cell-seeded hydrogels were imaged with a ZEISS Axio Observer Z1 inverted microscope. Lastly, cell viability was calculated as the ratio of live cells to the total number of cells using ImageJ software ($n = 4$).

2.8.5. Cell Adhesion and Spreading.—Cell spreading on the adhesive hydrogels was visualized by fluorescent staining of F-actin microfilaments and cell nuclei. Briefly, cell seeded hydrogels were fixed in 4% (v/v) paraformaldehyde (Sigma-Aldrich) for 20 min, and washed three times with DPBS at days 1, 3, and 5 postseeding. Samples were then permeabilized in 0.1% (w/v) Triton X-100 (Sigma) in DPBS for 20 min. Next, samples were incubated with Alexa-fluor 488-labeled rhodamine-phalloidin (2.5% (v/v) in 0.1% BSA, Invitrogen) for 45 min. Samples were washed three times with DPBS, and stained again with 1 μL/ml DAPI (4′,6-diamidino-2-phenylindole, Sigma-Aldrich) in DPBS for 5 min. Lastly, the cell seeded hydrogels were washed three times with DPBS and fluorescent image acquisition was carried out using an Axio Observer Z1 inverted microscope.

2.9. In Vitro Antimicrobial Activity of the Adhesive Hydrogels.

2.9.1. Methicillin-Resistant Staphylococcus aureus (MRSA) Seeding on Hydrogels.—MRSA (ATCC) was used to evaluate the in vitro antimicrobial properties of MeHA/ELP-ZnO hydrogels. MRSA stock cultures were hydrated and streaked for isolation on tryptic soy agar (Sigma). For all bacteria experiments, a single colony was used to inoculate 5 mL of tryptic soy broth (TSB; Sigma-Aldrich). The inoculated TSB was then placed on an incubator shaker set at 200 rpm for 18 h at 37 °C. The optical density of the bacteria suspension was then adjusted to 0.52 at 562 nm, which corresponded to a cell density of 1×10^9 colony-forming units (CFU) per ml. Lastly, the resulting solution was serially diluted in TSB over a 3-log range to a density of 1×10^6 CFU/mL.

The engineered hydrogels containing 0, 0.1, and 0.2% (w/v) ZnO were placed in separate wells of a 48-well plate and sterilized under UV light. Each scaffold was then seeded with 1 mL of bacteria solution, and the plate was incubated at 37 °C and 5% CO_2 for 24 h. Following incubation, the scaffolds were transferred to a new well plate and washed 3 times with DPBS to remove any remaining bacteria from the hydrogels.

2.9.2. Colony-Forming Units (CFU) Assay.—MeHA/ELP and MeHA/ELP-ZnO hydrogels were seeded with MRSA and incubated as described before ($n = 3$). After incubation, hydrogels were retrieved from the well plate and placed in 1.5 mL microcentrifuge tubes with 1 mL DPBS. The samples were carefully handled during transfer to avoid disruption of the bacterial biofilms on the hydrogels. The hydrogels were then vortexed at 3000 rpm for 15 min to strip all adherent bacteria from the hydrogels into DPBS. The resulting suspension was then serially diluted in DPBS over a 3-log range and three 10 μL drops of each dilution were plated on tryptic soy agar.[49] After 24 h of incubation at 37 °C and 5% CO_2, the number of MRSA colonies that formed on each plate was counted and raw CFU totals were calculated based on the dilution factor.

2.9.3. BacLight Live/Dead Assay.—The engineered hydrogels were seeded with MRSA and incubated as described before. After incubation, the hydrogels were stained using BacLight Bacterial Viability kit (ThermoFisher) according to instructions from the manufacturer. Following staining, the samples were visualized using an Axio Observer Z1 inverted microscope ($n = 3$).

2.9.4. Scanning electron microscopy (SEM) Imaging of Bacterial Clusters on Adhesive Hydrogels.—MeHA/ELP hydrogels with and without ZnO were seeded with MRSA and incubated as described before. After incubation, the samples were fixed in 2.5% glutaraldehyde (Sigma-Aldrich) at 4 °C for 2 h and lyophilized for 48 h. Lastly, the samples were mounted on SEM stubs, sputter coated with 6 nm of gold/palladium, and visualized using a Hitachi S-4800 SEM ($n = 3$).

2.10. In Vivo Biodegradation and Biocompatibility.

All animal protocols were approved by the Institutional Animal Care and Use Committee (Protocol No. 15–1248R) at Northeastern University. Male Wistar rats (200–250 g) were purchased from Charles River Laboratories (Wilmington, MA, USA) and kept in the animal core facility at Northeastern University (Boston, MA, USA). Adhesive hydrogels (2% MeHA, 10% ELP) were prepared under sterile conditions in cylindrical (2 × 6 mm disks) molds. Anesthesia was induced by isoflurane (2–2.5%) inhalation, followed by SC buprenorphine (0.02 to 0.05 mg/kg). Six 8 mm incisions were created on the posterior dorsomedial skin of the animals, and lateral subcutaneous pockets were prepared by blunt dissection. Hydrogels were then implanted into the subcutaneous pockets, followed by suture and recovery from anesthesia. Implanted samples were retrieved with the adjacent tissues after euthanasia at days 3, 14, 28, and 56 post implantation. For biodegradation studies, the samples were carefully cleaned to remove the surrounding tissue and then washed three times with DPBS. The dimensions of the hydrogels (diameter and height) were measured using a digital caliper and the samples were lyophilized to measure the weight loss over time.

2.10.1. Histological and Immunohistofluorescent Evaluation of in Vivo Biocompatibility.—After explantation, the adhesive hydrogels were fixed, mounted, flash frozen, and cryosectioned as described before.[3] The slides were then stained for hematoxylin and eosin (H&E) staining (Sigma) according to manufacturer's instructions. Immunohistofluorescent staining was performed on cryosections according to a methodology previously described in the literature.[31,50]

Anti-CD3 [SP7] (ab16669) and anti-CD68 (ab125212) (Abcam) were used as primary antibodies. An Alexa Fluor 594-conjugated antibody (Invitrogen) was also used as the secondary antibody. All samples were then stained again using DAPI. Lastly, the fluorescent images were taken using an Axio Observer Z1 inverted microscope.

2.11. Statistical Analysis.

At least 3 samples were tested for all experiments, and all data were expressed as mean ± standard deviation (*$p < 0.05$, **$p < 0.01$, ***$p < 0.001$ and ****$p < 0.0001$). *t* test, one-

way, or two-way ANOVA followed by Tukey's test or Bonferroni test were performed where appropriate to measure statistical significance (GraphPad Prism 6.0, GraphPad Software).

3. RESULTS AND DISCUSSION

3.1. Synthesis of MeHA/ELP Hybrid Hydrogels.

In contrast to hydrogels synthesized from a single polymer network, hybrid hydrogels have been shown to better mimic the multifunctional nature of native physiological microenvironments.[51] Furthermore, the combination of different polymers with distinct physicochemical properties enables the fine-tuning of the physical and biological properties of the engineered hydrogels.[52] In recent years, both MeHA and ELPs have emerged as remarkably promising biomaterials for various tissue engineering applications, including cartilage repair. Since both MeHA and ELPs are derived from naturally occurring polymers, they mimic the composition of the native ECM and provide biologically relevant cues to cells in vitro. The genetically encoded design of ELPs allows the modulation of the physical characteristics of the engineered tissue constructs.[29] Moreover, HA hydrogels have been shown to promote the deposition of cartilage-like ECM by chondrocytes and stem cells from different origins in vitro.[39,53] Despite the remarkable chondroinductive properties of HA-based hydrogels, their uncontrolled in vivo degradation rate and poor elasticity often limit their application for cartilage tissue regeneration and repair.[39,40] Therefore, we hypothesized that the incorporation of highly elastic ELPs into HA-based hydrogels could enhance the elasticity and resilience of the hydrogels, and improve their efficacy for cartilage repair. In addition, due to the slow in vivo degradation rate of ELP hydrogels,[31] we anticipated that the addition of ELP could be used to modulate the biodegradation of the scaffolds in vivo.

Light-controlled radical polymerization is one of the most widely used methods for the local delivery of hydrogels for tissue engineering applications.[46,54] In contrast to alternate cross-linking methods, such as chemical polymerization, the use of light enables precise control over hydrogel formation, modification, shape, and the induction of specific responses in smart biomaterials.[55] In addition, because of the fast reactivity of methacrylate groups with radicals, they are one of the most commonly utilized functional groups for radical polymerization.[56]

Here, we synthesized MeHA by adding methacrylic anhydride to HA under basic conditions, which is one of the simplest and most widely used chemistries to generate MeHA (Figure 1a).[57] We then synthesized and purified a highly elastic photo-cross-linkable ELP, based on a methodology described in our previous study.[31] We have demonstrated that hydrogels based on this specific ELP sequence exhibited high elasticity, long-term structural stability, and adequate host integration in vivo, without eliciting significant inflammatory responses.[31] The presence of thiol groups from cysteine residues in this ELP sequence allows for the formation of disulfide bonds and rapid photo-cross-linking upon exposure to UV light (Figure 1b). MeHA/ELP hydrogel precursors were prepared by combining different concentrations of MeHA (1 and 2% (w/v)) and ELP (0, 5, 10 and 15% (w/v)) with a 0.5% (w/v) solution of Irgacure 2959 as a photoinitiator in distilled water at 4 °C. To form MeHA/ELP hydrogels, the precursors were exposed to UV light for 120 s. Upon exposure to UV light, the methacrylated groups in MeHA reacted with the thiol

(-SH) groups in the cysteine residues of the ELPs as well as with themselves, which led to rapid photo-cross-linking and formation of a 3D hydrogel network[31,56] (Figure 1c). In addition, because the phase transition temperature of the synthesized ELP is above room temperature (28–29 °C) based on rheological characterization of the material with changes in temperature (Figure 1d), the MeHA/ELP precursor did not form insoluble aggregates prior to cross-linking and hydrogel formation. Therefore, MeHA/ELP prepolymers can be readily delivered to the affected area, and rapidly cross-linked in situ upon exposure to light in a controlled manner to form a porous scaffold (Figure 1e). In contrast, previous studies of hybrid HA/ELP hydrogels were hindered by comparatively more complex synthesis and limited processability.[23,41] For instance, Zhu et al. recently described the synthesis of a HA/ELP hybrid hydrogel for cartilage regeneration, in which the ELP required a time-consuming (>20 days) chemical modification process with hydrazine groups to render it reactive with aldehyde-modified HA.[41] In addition, the gelation process occurred very rapidly upon mixing the two components, which may cause operation complications, such as applicator nozzle clogging, in a clinical surgery setting. In another study, Moss et al. also described the engineering of a HA/ELP hybrid hydrogel, which required the incorporation of a third polymer (i.e., PEG diacrylate, PEGDA) as a cross-linker between the ELP and the thiol-modified HA to reduce the cross-linking time (10–15 min).[23] In contrast, the photo-cross-linkable MeHA/ELP prepolymers presented in this study required minor or no chemical modification. Furthermore, they can be readily delivered to the affected area as a liquid and rapidly cross-linked in situ upon exposure to UV light with control over the gelation kinetics. Overall, facile and comparatively fast chemical synthesis combined with the high adhesion properties of the MeHA/ELP-ZnO composite, convenience of the application process, and control over cross-linking greatly increases the potential for clinical translation of MeHA/ELP hydrogels for cartilage regeneration and repair.

3.2. Mechanical Characterization of the Composite Hydrogels.

In addition to biochemical stimuli, mechanical cues such as matrix stiffness and elasticity play a crucial role in the regulation of various cell processes and the promotion of new cartilage tissue formation.[24] Therefore, we characterized the mechanical properties of the engineered hydrogels synthesized with different concentrations of MeHA (i.e., 1 and 2% (w/v)) and ELP (i.e., 0, 5, 10, and 15% (w/v)) with and without ZnO nanoparticles using cyclic compression and tensile testing (Figure 2 and Figures S1 and S2). Our results suggest that the compressive modulus of MeHA/ELP hydrogels increased significantly by increasing ELP concentration from 0 to 10%, at both 1 and 2% MeHA concentrations (Figure 2a and Figure S1). For instance, for MeHA/ELP hydrogels containing 1% MeHA, the compressive modulus increased from 2.97 ± 2.5 kPa at 0% ELP to 13.1 ± 4.1 kPa at 10% ELP concentration (Figure 2a). In addition, the compressive modulus of MeHA/ELP hydrogels at 2% MeHA ranged from 14.8 ± 1.6 kPa to 39.9 ± 7.6 kPa by changing the ELP concentration from 0% to 10% (w/v) (Figure 2a). Previous studies have reported the engineering of chitosan/HA[58] and fibrin/HA scaffolds[59] with a maximum compressive modulus of 7 and 28 kPa, respectively. In addition, it was reported that the compressive moduli of hydrogels synthesized using different ELPs, such as ELP[KV7F-72][60] and ELP(KCTS-E 31-KCTS][31] were in the range of 4–11 and 5–14 kPa, respectively. Our results demonstrated that the compressive modulus of hybrid hydrogels synthesized using 10% ELP and 2% MeHA

(i.e., 39.9 ± 7.6 kPa) was higher than those observed in previous studies. This behavior could be explained due to the formation of an interpenetrating network between the MeHA and ELP polymers. Our results also demonstrated that the energy loss at cycle 8 for MeHA/ELP hydrogels increased from 18.8 ± 0.5% to 28.2 ± 2.7% for hydrogels with 1% MeHA, and from 3.4 ± 2.8 to 19.4 ± 3.3% for hydrogels with 2% MeHA by increasing ELP concentration (Figure 2b). Our previous work on ELP-based hydrogels demonstrated an energy loss of 35–51%[31] based on cyclic compression tests, which was remarkably higher than the values obtained for our MeHA/ELP composite hydrogels. The low energy dissipation during loading/unloading and high resilience of MeHA/ELP hydrogels highlight their potential for cartilage tissue repair. In addition, our results indicate that the compressive modulus of the adhesive hydrogels did not change by incorporation of antimicrobial ZnO nanoparticles at both 0.1 and 0.2%(w/v) concentrations (Figures 2c).

The results from tensile tests demonstrated that the elastic modulus, ultimate stress, and extensibility (ultimate strain) of MeHA/ELP hydrogels could also be tuned by varying the concentrations of MeHA and ELP (Figure 2d–e and Figure S2). The engineered hybrids exhibited highly tunable elastic moduli in the range of 1.6 ± 0.4 kPa to 8.8 ± 1.1 kPa for hydrogels with 1% MeHA, and 10.9 ± 4.9 kPa to 28.9 ± 2.9 kPa for hydrogels with 2% MeHA, by varying the ELP concentration (Figure 2d). In particular, hydrogels synthesized with 10% ELP and 2% MeHA exhibited the highest elastic modulus (i.e., 28.9 ± 2.9 kPa) (Figure 2d). Our results also showed that the ultimate stress of the engineered materials increased from 1.6 ± 0.0 kPa to 28.7 ± 4.8 kPa for hydrogels with 1% MeHA, when the ELP concentration increased from 0% to 10% (w/v) (Figure S2). In addition, the ultimate stress varied in the range of 4.7 ± 1.9 kPa to 20.3 ± 2.1 kPa for hydrogels synthesized with varying concentrations of ELP and 2% MeHA (Figure S2). Lastly, it was found that by increasing the ELP concentration from 0% to 15%, the extensibility of MeHA/ELP hybrids increased consistently from 70.9 ± 10.5% to 163.6 ± 11.4%, and from 40.9 ± 9.4% to 103.1 ± 10.3%, for hydrogels with 1% and 2% MeHA, respectively (Figure 2e). We observed a decrease in the elastic moduli of the hybrid hydrogels when the ELP concentration was increased from 10 to 15%, which was more significant at 2% MeHA concentration. However, hydrogel formulations with 15% ELP exhibited more elastic behavior, as demonstrated by their increased extensibility (Figure 2e). We hypothesize that this high concentration of ELP (15%) could enhance the elasticity of the resulting hybrid hydrogel but also make them soft. Similar to compressive properties, the tensile properties of the engineered hydrogels did not change significantly by incorporation of various concentrations of ZnO nanoparticles (Figures 2f).

The mechanical properties of cartilage tissues vary substantially depending on the maturity of the organism, the distance from the articular surface, the development of disease, as well as during physiological compression and tension.[61] Therefore, materials used to engineer hydrogel scaffolds for cartilage tissue engineering should possess highly tunable mechanical properties to achieve significant clinical relevance. Our results demonstrated that the combination of different concentrations of MeHA and ELP yielded hydrogels with a wide range of highly tunable mechanical properties. Therefore, the remarkable tunability brought about by the incorporation of both biopolymers makes the hybrid hydrogels highly

promising biomaterials for engineering cartilage tissue constructs with different mechanical properties.

3.3. In Vitro Adhesive Properties of MeHA/ELP Hydrogels.

High adhesion of implanted biomaterials to the surrounding tissue in vivo can prevent them from detaching from the target site and may promote biointegration. An optimal tissue/biomaterial integration promotes biocompatibility and effective tissue regeneration under physiological conditions.[5] We evaluated the in vitro adhesive properties of MeHA/ELP hydrogels using standard burst pressure and lap shear tests, and compared them to those of commercially available adhesives, Evicel and Coseal (Figure 3). These tests are particularly important to show the potential integration of adhesive hydrogel to the host tissue.[21] MeHA/ELP and MeHA/ELP-ZnO hydrogels showed consistently higher burst pressure values than commercially available sealants, as show in Figure 3a–c. As expected, burst pressure increased with increasing concentrations of MeHA, with the highest burst pressure observed for hydrogels containing 2% MeHA and 10% ELP (19.87 ± 6.92 kPa). Furthermore, this value was nearly 13 times greater than the burst pressure obtained when using Evicel (1.54 ± 0.99 kPa) and Coseal (1.68 ± 0.11 kPa) (Figure 2b). Additionally, the incorporation of ZnO nanoparticles had no significant effect on the burst pressure resistant of the engineered adhesives (Figure 2c). The high burst pressure obtained for the engineered hydrogel adhesives is particularly important for cartilage tissue engineering, because it confirms that the hydrogels are able to tolerate in vivo intra-articular pressures.[21] In addition to orthogonal forces, tangential forces are applied in the actual in vivo conditions. It is expected that the MeHA/ELP-ZnO adhesive hydrogels would exhibit significant resistance against intra-articular pressures in vivo, because of their high burst pressure. However, further confirmation through animal experiments would be necessary.[5,21]

In agreement with the results of the burst pressure tests, the lap shear experiments indicated that the shear strength of the hydrogels increased with increasing concentrations of MeHA (Figure 2d–f). Hydrogels containing 2% MeHA and 10% ELP exhibited the highest shear strength (443.1 ± 55.2 kPa), which constituted a 2-fold increase relative to Evicel and a > 6-fold increase relative to Coseal (Figure 2e). Furthermore, addition of ZnO nanoparticles did not change the shear strength of the engineered composite hydrogels (Figure 2f). The high burst pressure and shear strength of hydrogels containing 2% MeHA, 10% ELP, and 0.2% ZnO highlight their potential to be used as bioadhesives for different applications. Particularly, due to the mechanically harsh environment of the joints and presence of physiological shear stresses and loads in cartilage sites,[5] it is expected that MeHA/ELP-ZnO adhesive hydrogels can better adhere to and integrate with the native tissues as compared to those commercial available adhesive materials.

3.4. Swelling Ratios of MeHA/ELP Hybrid Hydrogels.

Another important property of hydrogel scaffolds is their ability to undergo volumetric changes, in response to increased water uptake in physiological wet tissues. Therefore, we evaluated the swellability of MeHA/ELP hydrogels, by incubating them in DPBS at 37 °C for 24 h (Figures S3). Our results demonstrated that the maximum swelling was consistently obtained in all samples at 2 h postincubation, with no significant changes until

24 h of incubation (Figures S3a and S3b). In addition, our results also showed that the swellability of the hydrogels was significantly decreased because of the incorporation of ELP in hydrogels for both 1% (Figure S3a) and 2% (Figure S3b) MeHA concentrations. For example, the swelling ratios of hydrogels with 1% MeHA decreased from 3804 ± 1030% to 484 ± 76% by increasing ELP concentration from 0% to 15%. This observation could be explained by the fact that ELP-based hydrogels contract and lose water content due to molecular rearrangement, at temperatures higher than their transition temperature.[62] Therefore, the combination of ELPs and MeHA could be used to modulate the water uptake capacity of hybrid hydrogels.

The tunable water uptake capacity of MeHA/ELP hydrogels allows the tuning of the microstructure of the scaffold to promote cell penetration and new autologous tissue ingrowth, as well as proper vascularization and nutrient diffusion.[63] In addition, previous works have demonstrated that a higher degree of swellability could help promote cartilaginous ECM deposition, but could also impact the mechanical properties of the scaffolds.[64] This characteristic is particularly important in the context of articular cartilage, due to its paramount role in mechanical support and load bearing in articular joints.[11] Furthermore, previous groups have also demonstrated that the swellability of the hydrogels also influences their potential to induce chondrogenic differentiation in 3D encapsulated hMSCs.[65]

3.5. In Vitro Cytocompatibility of the Engineered Composite Hydrogels.

Bioactive scaffolds used for tissue engineering applications not only provide physical support, but they also influence cell survival through their interactions with different cell membrane receptors.[66] Different properties of hydrogel scaffolds have been shown to affect cell viability and proliferation, including material chemistry and functionalization with bioactive motifs, the addition of soluble autocrine factors, as well as nutrient and oxygen diffusion. Thus, we characterized the in vitro cytocompatibility of the engineered MeHA/ELP-ZnO hydrogels using two cell lines, hMSCs (Figure 4) and NIH-3T3 cells (Figure S4).

We evaluated the ability of hMSCs and NIH-3T3 fibroblasts to grow on the surface of MeHA/ELP hydrogels synthesized with 2% MeHA and 10% ELP concentrations, with and without ZnO nanoparticles (Figure 4 and Figure S4). The in vitro cytocompatibility of MeHA/ELP (control) and MeHA/ELP-ZnO composite hydrogels was evaluated using commercial live/dead and PrestoBlue assays, as well as Actin/DAPI fluorescent staining. These results demonstrated that both MeHA/ELP and MeHA/ELP-ZnO composite hydrogels could support the proliferation and spreading of metabolically active cells, which is critical for their implementation in tissue engineering applications. For example, hMSCs seeded on the surface of the engineered hydrogels showed high cell viabilities (>90%) (Figure 4a, b, e) and spreading (Figure 4c, d) during the first 5 days of culture. Furthermore, the presence of 0.2%(w/v) ZnO nanoparticles did not affect the cytocompatibility of the gels seeded with hMSCs at day 5 post cell seeding (Figure 4e). In addition, our results demonstrated that the metabolic activity (i.e., relative fluorescence units, RFUs) of hMSCs increased more than 2.3- and 2.7-fold from day 1 to day 5 after cell seeding for control samples (0% ZnO) and MeHA/ELP-ZnO, respectively (Figure 4f). In particular, the RFUs

of seeded hMSCs increased from 3549 ± 171 on day 1 to 8486 ± 1387 on day 5, which was not significantly different from hydrogels without ZnO as control (Figure 4f). Similar cell behaviors (viability, spreading and metabolic activity) were observed for the samples seeded with NIH-3T3 fibroblast cells (Figure S4). For instance, more than 90% of the NIH-3T3 cells were viable after 5 days of seeding on adhesive hydrogels (Figure S4a, b, e). In addition, fibroblasts seeded on adhesive hydrogels showed high spreading (Figure S4c, d) and increased metabolic activity (>3-fold) during the experimental period (Figure S4f). Taken together, these results indicated that the adhesive composite hydrogels could support the growth and proliferation of metabolically active cells in vitro.

Previous studies have explored the use of ECM-derived polymers to engineer scaffolds for cartilage tissue engineering, as well as for chondrocyte delivery for cartilage repair. For instance, some studies have explored the influence of scaffold chemistry in chondrogenesis, by encapsulating hMSCs in HA-based hydrogels.[40,67,68] However, these approaches required prolonged exposure times to UV light (10 min), which could potentially lead to decreased cell viability or DNA damage. In contrast, MeHA/ELP hydrogels can be rapidly cross-linked, which greatly minimizes biosafety concerns associated with UV-based chemistries. In addition, the incorporation of ELPs into MeHA/ELP hydrogels synergizes the bioactivity of the scaffolds, while also enabling the fine-tuning of their physical properties.

3.6. In Vitro Antibacterial Properties of the Hybrid Hydrogels.

The development of infection still constitutes one of the most severe postoperative complications in clinical orthopedics. Infections occur because of bacterial adhesion and colonization across the surface of implanted biomaterials, which ultimately leads to the formation of a biofilm that protects pathogenic bacteria against phagocytosis and antibiotics.[6] In addition, the misuse and over prescription of antibiotics have led to the development of antibiotic-resistant bacteria. Therefore, significant efforts have been made toward the development of antimicrobial hydrogels that can prevent biofilm formation and implant rejection.[69,70] One of the most promising experimental strategies for overcoming antibiotic resistance in pathogenic bacteria is the use of nanoparticle-based alternatives. For instance, ZnO nanoparticles have been shown to elicit antimicrobial activity against antibiotic-resistant bacteria, through the disruption of bacterial cell membranes and the induction of reactive oxygen species.[43]

Here, we incorporated different concentrations of ZnO nanoparticles (0, 0.1, and 0.2% (w/v)) to impart antimicrobial properties to MeHA/ELP hydrogels synthesized using 2% MeHA and 10% ELP concentrations. We investigated the antimicrobial activity of the resulting MeHA/ELP-ZnO nanocomposites against MRSA. For this, we relied on direct visual inspection of the hydrogels seeded with bacteria via SEM, as well as colony forming units (CFU) and live/dead assays. SEM micrographs showed that the samples containing 0.0% ZnO (controls) exhibited extensive bacterial infiltration within the pores, as well as across the surface of the scaffolds (Figure 5a, b). The incorporation of 0.1% ZnO into the hydrogel network provided limited protection against MRSA colonization, as shown by the persistence of bacterial clusters located mostly on the surface of the scaffolds (Figure 5c, d).

In contrast, hybrid hydrogels containing 0.2% ZnO exhibited high antimicrobial activity as demonstrated by the complete absence of bacterial clusters both inside and on the surface of scaffolds (Figure 5e, f). We then evaluated bacterial cell viability within MeHA/ELP-ZnO hydrogels using the BacLight live/dead cell viability assay (Figure 5g–i). Fluorescent images suggested that the number of viable (green) bacterial cells inside the hydrogels decreased via the incorporation of 0.1 and 0.2% ZnO, when compared to control hydrogels (without ZnO) (Figure 5g–i). These observations were further supported by the CFU assay, which showed that the number of CFUs decreased from 40.7 ± 8.1 at 0.0% ZnO, to 38.3 ± 5.5 at 0.1% ZnO and 28.3 ± 4.7 at 0.2% ZnO concentration (Figure 5j).

Previous studies have reported the incorporation of ZnO nanoparticles into chitosan and alginate-based hydrogels to impart antimicrobial properties.[45,71] However, the incorporation of metal oxide nanoparticles into these types of hydrogels has been shown to exert a negative effect on cell viability. For instance, Mohandas et al. reported a > 2-fold reduction in cell viability after the addition of ZnO nanoparticles to alginate hydrogels.[45] In contrast, our results demonstrated that MeHA/ELP-ZnO hydrogels exhibited high antimicrobial activity, without compromising cell viability and spreading (Figures 4 and Figure S4). In addition, our findings showed that the incorporation of ZnO nanoparticles resulted in no significant changes in the elastic and compressive moduli as well as adhesive properties of MeHA/ELP hydrogels (Figure 2c, f). Taken together, these results demonstrated that MeHA/ELP-ZnO hydrogels could be effectively implemented in the engineering of adhesive hydrogels that are resistant to bacterial colonization.

3.7. In Vivo Biodegradation and Biocompatibility of the Engineered MeHA/ELP Hybrid Hydrogels.

Hydrogels used for tissue engineering applications should not induce inflammatory or foreign body responses when surgically implanted in vivo.[31] In addition, they should be effectively biodegraded into biocompatible byproducts, while allowing sufficient time for tissue regeneration. Thus, we evaluated the in vivo biodegradation and biocompatibility of MeHA/ELP hydrogels via subcutaneous implantation in rats. For this, cylindrical (8 mm diameter by 2 mm height) hydrogels were synthesized using 2% MeHA and 10% ELP concentrations. Hydrogels were lyophilized and weighed, and the dried samples were then subcutaneously implanted in the dorsum of male Wistar rats. Implanted samples were retrieved and weighed 3, 14, 28, and 56 days post implantation, and analyzed via direct visual inspection, and histological and immunofluorescent staining. Visual inspection of the explanted samples showed that the average volume of the hydrogels decreased significantly throughout the duration of the experiment (69 ± 11% after 56 days) (Figure 6a, b). This change in the volume of the samples was likely due to the biodegradation of the hydrogels via enzymatic hydrolysis.[31]

The average degradation based on the weight of the explanted samples also increased from 25.2 ± 3.9% at day 14 to 42.7 ± 7.5% at day 28 and dropped to 21.2 ± 7.2% on day 56 post implantation (Figure 6b). This decrease in the degradation rate might be due to the ingrowth of new autologous tissue within the engineered hydrogels, which led to an increase in the weight of the explanted sample on day 56 (Figure 6b). This observation

was also apparent after visual inspection of the explanted samples (Figure 6a). These results were in agreement with our previous work, which demonstrated that ELP implants allowed the ingrowth of predominantly noninflammatory tissue into the scaffold.[31] The efficient control over the biodegradation rate of the hydrogels enables their fine-tuning for different tissue engineering applications. Previous studies have demonstrated that both MeHA[72,73] and ELP[29,74,75] can be effectively biodegraded in vivo, and that the rate at which this process occurs can be controlled by modifying their biochemical composition. These observations suggest that the biodegradability of the hybrid hydrogels can be finely tuned not only by varying the concentration of MeHA and ELP biopolymers, but also by further modifying their biochemical structure. Therefore, the tunable biodegradability of MeHA/ELP hydrogels could prove greatly advantageous for the engineering of biomaterials for different biomedical and tissue engineering applications.

Lastly, we evaluated the immunogenicity of the engineered hydrogels, via histological and immunohistochemical analysis of subcutaneously implanted samples. H&E staining revealed that the hybrid hydrogels were efficiently biodegraded and replaced by new autologous tissue, without any apparent signs of fibrous capsule formation (Figure 6c–e). The degree of inflammatory cell recruitment around the hydrogel was evaluated via immunofluorescent staining using antibodies against the lymphocyte (CD3) and macrophage (CD68) associated antigens. These results showed no detectable lymphocyte invasion (CD3, red) throughout the duration of the experiment (56 days) (Figure 6f–h). In addition, immunofluorescent staining against the CD68 antigen showed minor macrophage infiltration at day 4 post implantation (Figure 6i). However, we did not detect any observable fluorescence for the CD68 antigen at days 28 and 56 post implantation (Figure 6j, k). These results indicate that MeHA/ELP hydrogels possess high biocompatibility in vivo, as demonstrated by the absence of any sustained inflammatory responses from the host organism. Taken together, these observations suggest that the engineered hybrid hydrogels can be used for tissue engineering applications, due to their tunable biodegradability and high biocompatibility.

4. CONCLUSION

In this study, we engineered a new class of MeHA/ELP bioactive hydrogels with antimicrobial and adhesive properties for different tissue engineering applications in particular cartilage repair. MeHA/ELP hydrogels exhibited a wide range of highly tunable physical properties, including mechanical strength, elasticity, adhesion strength, and swellability. Standard lap shear and burst pressure tests revealed that MeHA/ELP hydrogels exhibited higher adhesive strength, compared to commercially available tissue adhesives such as Evicel and Coseal. In vitro studies also demonstrated that the engineered hydrogels were cytocompatible and could promote the proliferation and spreading of hMSCs as well as NIH-3T3 cells. In addition, the incorporation of ZnO nanoparticles into MeHA/ELP hydrogels provided high antimicrobial activity against MRSA in vitro. In vivo subcutaneous implantation showed that the engineered hydrogels could be biodegraded and integrated into the host surrounding tissues, without eliciting any significant inflammatory responses. Taken together, our results suggest that MeHA/ELP-ZnO hydrogels have the potential to be

used for different tissue engineering applications, especially cartilage repair, because of their tunable physical and mechanical properties, as well as antimicrobial properties.

Supplementary Material

Refer to Web version on PubMed Central for supplementary material.

ACKNOWLEDGMENTS

N.A. acknowledges the support from the American Heart Association (AHA, 16SDG31280010), National Institutes of Health (NIH) (R01EB023052; R01HL140618), NIH-Center for Dental, Oral & Craniofacial Tissue & Organ Regeneration (C-DOCTOR), and Northeastern University.

REFERENCES

1. Jia X; Kiick KL Hybrid multicomponent hydrogels for tissue engineering. Macromol. Biosci. 2009, 9 (2), 140–56. [PubMed: 19107720]
2. Annabi N; Tamayol A; Uquillas JA; Akbari M; Bertassoni LE; Cha C; Camci-Unal G; Dokmeci MR; Peppas NA; Khademhosseini A 25th anniversary article: Rational design and applications of hydrogels in regenerative medicine. Adv. Mater. 2014, 26 (1), 85–123. [PubMed: 24741694]
3. Annabi N; Rana D; Shirzaei Sani E; Portillo-Lara R; Gifford JL; Fares MM; Mithieux SM; Weiss AS Engineering a sprayable and elastic hydrogel adhesive with antimicrobial properties for wound healing. Biomaterials 2017, 139, 229243. [PubMed: 28579065]
4. Assmann A; Vegh A; Ghasemi-Rad M; Bagherifard S; Cheng G; Sani ES; Ruiz-Esparza GU; Noshadi I; Lassaletta AD; Gangadharan S; Tamayol A; Khademhosseini A; Annabi N A highly adhesive and naturally derived sealant. Biomaterials 2017, 140, 115–127. [PubMed: 28646685]
5. Wang DA; Varghese S; Sharma B; Strehin I; Fermanian S; Gorham J; Fairbrother DH; Cascio B; Elisseeff JH Multifunctional chondroitin sulphate for cartilage tissue-biomaterial integration. Nat. Mater. 2007, 6 (5), 385–92. [PubMed: 17435762]
6. Drago L; Boot W; Dimas K; Malizos K; Hänsch GM; Stuyck J; Gawlitta D; Romanó CL Does Implant Coating With Antibacterial-Loaded Hydrogel Reduce Bacterial Colonization and Biofilm Formation in Vitro? Clin. Orthop. Relat. Res. 2014, 472 (11), 3311–3323. [PubMed: 24622801]
7. Sharma B; Fermanian S; Gibson M; Unterman S; Herzka DA; Cascio B; Coburn J; Hui AY; Marcus N; Gold GE; Elisseeff JH Human cartilage repair with a photoreactive adhesive-hydrogel composite. Sci. Transl. Med. 2013, 5 (167), 167ra6–167ra6.
8. Chuah YJ; Peck Y; Lau JE; Hee HT; Wang DA Hydrogel based cartilaginous tissue regeneration: recent insights and technologies. Biomater. Sci. 2017, 5, 613. [PubMed: 28233881]
9. Tan H; Chu CR; Payne KA; Marra KG Injectable in situ forming biodegradable chitosan-hyaluronic acid based hydrogels for cartilage tissue engineering. Biomaterials 2009, 30 (13), 2499–506. [PubMed: 19167750]
10. Hoemann CD; Sun J; Légaré A; McKee MD; Buschmann MD Tissue engineering of cartilage using an injectable and adhesive chitosan-based cell-delivery vehicle. Osteoarthritis and Cartilage 2005, 13 (4), 318–329. [PubMed: 15780645]
11. Kim IL; Mauck RL; Burdick JA Hydrogel design for cartilage tissue engineering: a case study with hyaluronic acid. Biomaterials 2011, 32 (34), 8771–82. [PubMed: 21903262]
12. Levett PA; Melchels FP; Schrobback K; Hutmacher DW; Malda J; Klein TJ A biomimetic extracellular matrix for cartilage tissue engineering centered on photocurable gelatin, hyaluronic acid and chondroitin sulfate. Acta Biomater. 2014, 10 (1), 214–23. [PubMed: 24140603]
13. Chen WH; Lo WC; Hsu WC; Wei HJ; Liu HY; Lee CH; Tina Chen SY; Shieh YH; Williams DF; Deng WP Synergistic anabolic actions of hyaluronic acid and platelet-rich plasma on cartilage regeneration in osteoarthritis therapy. Biomaterials 2014, 35 (36), 9599–607. [PubMed: 25176059]
14. Lee P; Tran K; Chang W; Shelke NB; Kumbar SG; Yu X Influence of chondroitin sulfate and hyaluronic acid presence in nanofibers and its alignment on the bone marrow stromal cells: cartilage regeneration. J. Biomed. Nanotechnol. 2014, 10 (8), 1469–79. [PubMed: 25016647]

15. Skaalure SC; Dimson SO; Pennington AM; Bryant SJ Semi-interpenetrating networks of hyaluronic acid in degradable PEG hydrogels for cartilage tissue engineering. Acta Biomater. 2014, 10 (8), 3409–20. [PubMed: 24769116]
16. Yodmuang S; McNamara SL; Nover AB; Mandal BB; Agarwal M; Kelly TA; Chao PH; Hung C; Kaplan DL; Vunjak-Novakovic G Silk microfiber-reinforced silk hydrogel composites for functional cartilage tissue repair. Acta Biomater. 2015, 11, 27–36. [PubMed: 25281788]
17. Singh YP; Bhardwaj N; Mandal BB Potential of Agarose/Silk Fibroin Blended Hydrogel for in Vitro Cartilage Tissue Engineering. ACS Appl. Mater. Interfaces 2016, 8 (33), 21236–49. [PubMed: 27459679]
18. Chao PH; Yodmuang S; Wang X; Sun L; Kaplan DL; Vunjak-Novakovic G Silk hydrogel for cartilage tissue engineering. J. Biomed. Mater. Res., Part B 2010, 95 (1), 84–90.
19. Kontturi LS; Jarvinen E; Muhonen V; Collin EC; Pandit AS; Kiviranta I; Yliperttula M; Urtti A An injectable, in situ forming type II collagen/hyaluronic acid hydrogel vehicle for chondrocyte delivery in cartilage tissue engineering. Drug Delivery Transl. Res. 2014, 4 (2), 149–58.
20. Parmar PA; Chow LW; St-Pierre JP; Horejs CM; Peng YY; Werkmeister JA; Ramshaw JA; Stevens MM Collagen-mimetic peptide-modifiable hydrogels for articular cartilage regeneration. Biomaterials 2015, 54, 213–25. [PubMed: 25907054]
21. Balakrishnan B; Joshi N; Jayakrishnan A; Banerjee R Self-crosslinked oxidized alginate/gelatin hydrogel as injectable, adhesive biomimetic scaffolds for cartilage regeneration. Acta Biomater. 2014, 10 (8), 3650–3663. [PubMed: 24811827]
22. Park H; Lee KY Facile control of RGD-alginate/hyaluronate hydrogel formation for cartilage regeneration. Carbohydr. Polym. 2011, 86 (3), 1107–1112.
23. Moss IL; Gordon L; Woodhouse KA; Whyne CM; Yee AJM A Novel Thiol-Modified Hyaluronan and Elastin-Like Polypetide Composite Material for Tissue Engineering of the Nucleus Pulposus of the Intervertebral Disc. Spine 2011, 36 (13), 1022–1029. [PubMed: 21150701]
24. Yang J; Zhang YS; Yue K; Khademhosseini A Cell-Laden Hydrogels for Osteochondral and Cartilage Tissue Engineering. Acta Biomater. 2017, 57, 1. [PubMed: 28088667]
25. Liao J; Shi K; Ding Q; Qu Y; Luo F; Qian Z Recent developments in scaffold-guided cartilage tissue regeneration. J. Biomed. Nanotechnol. 2014, 10 (10), 3085–104. [PubMed: 25992430]
26. McHale MK; Setton LA; Chilkoti A Synthesis and in Vitro Evaluation of Enzymatically Cross-Linked Elastin-Like Polypeptide Gels for Cartilaginous Tissue Repair. Tissue Eng. 2005, 11 (11–12), 1768–1779. [PubMed: 16411822]
27. Betre H; Setton LA; Meyer DE; Chilkoti A Characterization of a genetically engineered elastin-like polypeptide for cartilaginous tissue repair. Biomacromolecules 2002, 3 (5), 910–6. [PubMed: 12217035]
28. McHale MK; Setton LA; Chilkoti A Synthesis and in vitro evaluation of enzymatically cross-linked elastin-like polypeptide gels for cartilaginous tissue repair. Tissue Eng. 2005, 11 (11–12), 1768–79. [PubMed: 16411822]
29. MacEwan SR; Chilkoti A Elastin-like polypeptides: biomedical applications of tunable biopolymers. Biopolymers 2010, 94 (1), 60–77. [PubMed: 20091871]
30. Moss IL; Gordon L; Woodhouse KA; Whyne CM; Yee AJ A novel thiol-modified hyaluronan and elastin-like polypetide composite material for tissue engineering of the nucleus pulposus of the intervertebral disc. Spine (Philadelphia) 2011, 36 (13), 1022–9.
31. Zhang YN; Avery RK; Vallmajo-Martin Q; Assmann A; Vegh A; Memic A; Olsen BD; Annabi N; Khademhosseini A A Highly Elastic and Rapidly Crosslinkable Elastin-Like Polypeptide-Based Hydrogel for Biomedical Applications. Adv. Funct. Mater. 2015, 25 (30), 4814–4826. [PubMed: 26523134]
32. Collins MN; Birkinshaw C Hyaluronic acid based scaffolds for tissue engineering–a review. Carbohydr. Polym. 2013, 92 (2), 1262–79. [PubMed: 23399155]
33. Yoon IS; Chung CW; Sung JH; Cho HJ; Kim JS; Shim WS; Shim CK; Chung SJ; Kim DD Proliferation and chondrogenic differentiation of human adipose-derived mesenchymal stem cells in porous hyaluronic acid scaffold. J. Biosci. Bioeng. 2011, 112 (4), 402–8. [PubMed: 21802988]

34. Kim IL; Khetan S; Baker BM; Chen CS; Burdick JA Fibrous hyaluronic acid hydrogels that direct MSC chondrogenesis through mechanical and adhesive cues. Biomaterials 2013, 34 (22), 5571–5580. [PubMed: 23623322]
35. Sato E; Ando T; Ichikawa J; Okita G; Sato N; Wako M; Ohba T; Ochiai S; Hagino T; Jacobson R; Haro H High molecular weight hyaluronic acid increases the differentiation potential of the murine chondrocytic ATDC5 cell line. J. Orthop. Res. 2014, 32 (12), 1619–27. [PubMed: 25196420]
36. Matsiko A; Levingstone TJ; O'Brien FJ; Gleeson JP Addition of hyaluronic acid improves cellular infiltration and promotes early-stage chondrogenesis in a collagen-based scaffold for cartilage tissue engineering. Journal of the mechanical behavior of biomedical materials 2012, 11, 41–52. [PubMed: 22658153]
37. Hillel AT; Unterman S; Nahas Z; Reid B; Coburn JM; Axelman J; Chae JJ; Guo Q; Trow R; Thomas A; et al. Photoactivated composite biomaterial for soft tissue restoration in rodents and in humans. Sci. Transl. Med. 2011, 3 (93), 93ra67–93ra67.
38. Pitarresi G; Palumbo FS; Calascibetta F; Fiorica C; Di Stefano M; Giammona G Medicated hydrogels of hyaluronic acid derivatives for use in orthopedic field. Int. J. Pharm. 2013, 449 (1–2), 84–94. [PubMed: 23587968]
39. Chung C; Mesa J; Randolph MA; Yaremchuk M; Burdick JA Influence of gel properties on neocartilage formation by auricular chondrocytes photoencapsulated in hyaluronic acid networks. J. Biomed. Mater. Res., Part A 2006, 77 (3), 518–525.
40. Bian L; Hou C; Tous E; Rai R; Mauck RL; Burdick JA The influence of hyaluronic acid hydrogel crosslinking density and macromolecular diffusivity on human MSC chondrogenesis and hypertrophy. Biomaterials 2013, 34 (2), 413–21. [PubMed: 23084553]
41. Zhu D; Wang H; Trinh P; Heilshorn SC; Yang F Elastin-like protein-hyaluronic acid (ELP-HA) hydrogels with decoupled mechanical and biochemical cues for cartilage regeneration. Biomaterials 2017, 127, 132–140. [PubMed: 28268018]
42. Bernhard JC; Vunjak-Novakovic G Should we use cells, biomaterials, or tissue engineering for cartilage regeneration? Stem Cell Res. Ther. 2016, 7, No. 56. [PubMed: 27089917]
43. Pelgrift RY; Friedman AJ Nanotechnology as a therapeutic tool to combat microbial resistance. Adv. Drug Delivery Rev. 2013, 65 (13–14), 1803–1815.
44. Sharma RK; Balani K Mechanics of ZnO micro-rod and ZnO nanoparticle reinforcement in ultra-high molecular weight polyethylene biocomposite. J. Phys. D: Appl. Phys. 2014, 47 (34), 345301.
45. Mohandas A; Sudheesh Kumar PT; Raja B; Lakshmanan V-K; Jayakumar R. Exploration of alginate hydrogel/nano zinc oxide composite bandages for infected wounds. Int. J. Nanomed. 2015, 10 (Suppl 1), 53–66.
46. Smeds KA; Pfister-Serres A; Miki D; Dastgheib K; Inoue M; Hatchell DL; Grinstaff MW Photocrosslinkable polysaccharides for in situ hydrogel formation. J. Biomed. Mater. Res. 2001, 54 (1), 115–121. [PubMed: 11077410]
47. Bian LM; Zhai DY; Tous E; Rai R; Mauck RL; Burdick JA Enhanced MSC chondrogenesis following delivery of TGF-beta 3 from alginate microspheres within hyaluronic acid hydrogels in vitro and in vivo. Biomaterials 2011, 32 (27), 6425–6434. [PubMed: 21652067]
48. Zhang YN; Avery RK; Vallmajo-Martin Q; Assmann A; Vegh A; Memic A; Olsen BD; Annabi N; Khademhosseini A A highly elastic and rapidly crosslinkable elastin-like polypeptide-based hydrogel for biomedical applications. Adv. Funct. Mater. 2015, 25 (30), 4814–4826. [PubMed: 26523134]
49. Chen CY; Nace GW; Irwin PLA 6 × 6 drop plate method for simultaneous colony counting and MPN enumeration of Campylobacter jejuni, Listeria monocytogenes, and Escherichia coli. J. Microbiol. Methods 2003, 55 (2), 475–9. [PubMed: 14529971]
50. Assmann A; Delfs C; Munakata H; Schiffer F; Horstkotter K; Huynh K; Barth M; Stoldt VR; Kamiya H; Boeken U; Lichtenberg A; Akhyari P Acceleration of autologous in vivo recellularization of decellularized aortic conduits by fibronectin surface coating. Biomaterials 2013, 34 (25), 6015–26. [PubMed: 23683757]
51. Lau HK; Kiick KL Opportunities for multicomponent hybrid hydrogels in biomedical applications. Biomacromolecules 2015, 16 (1), 28–42. [PubMed: 25426888]

52. Zhu Q; Jiang Y; Lin S; Wen L; Wu D; Zhao M; Chen F; Jia Y; Yang B Structural identification of (1–>6)-alpha-d-glucan, a key responsible for the health benefits of longan, and evaluation of anticancer activity. Biomacromolecules 2013, 14 (6), 1999–2003. [PubMed: 23617585]
53. Astachov L; Vago R; Aviv M; Nevo Z Hyaluronan and mesenchymal stem cells: from germ layer to cartilage and bone. Front. Biosci., Landmark Ed. 2011, 16, 261–76. [PubMed: 21196170]
54. Chen M; Zhong M; Johnson JA Light-Controlled Radical Polymerization: Mechanisms, Methods, and Applications. Chem. Rev. 2016, 116 (17), 10167–211. [PubMed: 26978484]
55. Chatani S; Kloxin CJ; Bowman CN The power of light in polymer science: photochemical processes to manipulate polymer formation, structure, and properties. Polym. Chem. 2014, 5 (7), 2187–2201.
56. Burdick JA; Prestwich GD Hyaluronic acid hydrogels for biomedical applications. Adv. Mater. 2011, 23 (12), H41. [PubMed: 21394792]
57. Burdick JA; Prestwich GD Hyaluronic acid hydrogels for biomedical applications. Adv. Mater. 2011, 23 (12), H41–56. [PubMed: 21394792]
58. Tan H; Chu CR; Payne KA; Marra KG Injectable in situ forming biodegradable chitosan–hyaluronic acid based hydrogels for cartilage tissue engineering. Biomaterials 2009, 30 (13), 2499–2506. [PubMed: 19167750]
59. Snyder TN; Madhavan K; Intrator M; Dregalla RC; Park D A fibrin/hyaluronic acid hydrogel for the delivery of mesenchymal stem cells and potential for articular cartilage repair. J. Biol. Eng. 2014, 8, 10. [PubMed: 25061479]
60. Lim DW; Nettles DL; Setton LA; Chilkoti A In situ cross-linking of elastin-like polypeptide block copolymers for tissue repair. Biomacromolecules 2008, 9 (1), 222–30. [PubMed: 18163573]
61. Nguyen QT; Hwang Y; Chen AC; Varghese S; Sah RL Cartilage-like mechanical properties of poly (ethylene glycol)-diacrylate hydrogels. Biomaterials 2012, 33 (28), 6682–90. [PubMed: 22749448]
62. Trabbic-Carlson K; Setton LA; Chilkoti A Swelling and mechanical behaviors of chemically cross-linked hydrogels of elastin-like polypeptides. Biomacromolecules 2003, 4 (3), 572–580. [PubMed: 12741772]
63. Martin L; Alonso M; Girotti A; Arias FJ; Rodriguez-Cabello JC Synthesis and characterization of macroporous thermosensitive hydrogels from recombinant elastin-like polymers. Biomacromolecules 2009, 10 (11), 3015–22. [PubMed: 19795832]
64. Liu H Nanocomposites for Musculoskeletal Tissue Regeneration; Elsevier Science: Amsterdam, 2016.
65. Park H; Guo X; Temenoff JS; Tabata Y; Caplan AI; Kasper FK; Mikos AG Effect of swelling ratio of injectable hydrogel composites on chondrogenic differentiation of encapsulated rabbit marrow mesenchymal stem cells in vitro. Biomacromolecules 2009, 10 (3), 541–6. [PubMed: 19173557]
66. Resende RR; Fonseca EA; Tonelli FM; Sousa BR; Santos AK; Gomes KN; Guatimosim S; Kihara AH; Ladeira LO Scale/topography of substrates surface resembling extracellular matrix for tissue engineering. J. Biomed. Nanotechnol. 2014, 10 (7), 1157–93. [PubMed: 24804539]
67. Chung C; Burdick JA Influence of three-dimensional hyaluronic acid microenvironments on mesenchymal stem cell chondrogenesis. Tissue Eng., Part A 2009, 15 (2), 243–54. [PubMed: 19193129]
68. Toh WS; Lim TC; Kurisawa M; Spector M Modulation of mesenchymal stem cell chondrogenesis in a tunable hyaluronic acid hydrogel microenvironment. Biomaterials 2012, 33 (15), 3835–45. [PubMed: 22369963]
69. Finnegan S; Percival SL Clinical and Antibiofilm Efficacy of Antimicrobial Hydrogels. Adv. Wound Care (New Rochelle) 2015, 4 (7), 398–406. [PubMed: 26155382]
70. Ng VW; Chan JM; Sardon H; Ono RJ; Garcia JM; Yang YY; Hedrick JL Antimicrobial hydrogels: a new weapon in the arsenal against multidrug-resistant infections. Adv. Drug Delivery Rev. 2014, 78, 46–62.
71. Sudheesh Kumar PT; Lakshmanan VK; Anilkumar TV; Ramya C; Reshmi P; Unnikrishnan AG; Nair SV; Jayakumar R Flexible and microporous chitosan hydrogel/nano ZnO composite bandages for wound dressing: in vitro and in vivo evaluation. ACS Appl. Mater. Interfaces 2012, 4 (5), 2618–2629. [PubMed: 22489770]

72. Chung C; Beecham M; Mauck RL; Burdick JA The influence of degradation characteristics of hyaluronic acid hydrogels on in vitro neocartilage formation by mesenchymal stem cells. Biomaterials 2009, 30 (26), 4287–96. [PubMed: 19464053]

73. Sahoo S; Chung C; Khetan S; Burdick JA Hydrolytically degradable hyaluronic acid hydrogels with controlled temporal structures. Biomacromolecules 2008, 9 (4), 1088–92. [PubMed: 18324776]

74. Liu W; Dreher MR; Furgeson DY; Peixoto KV; Yuan H; Zalutsky MR; Chilkoti A Tumor accumulation, degradation and pharmacokinetics of elastin-like polypeptides in nude mice. J. Controlled Release 2006, 116 (2), 170–8.

75. Shamji MF; Whitlatch L; Friedman AH; Richardson WJ; Chilkoti A; Setton LA An injectable and in situ-gelling biopolymer for sustained drug release following perineural administration. Spine (Philadelphia) 2008, 33 (7), 748–54.

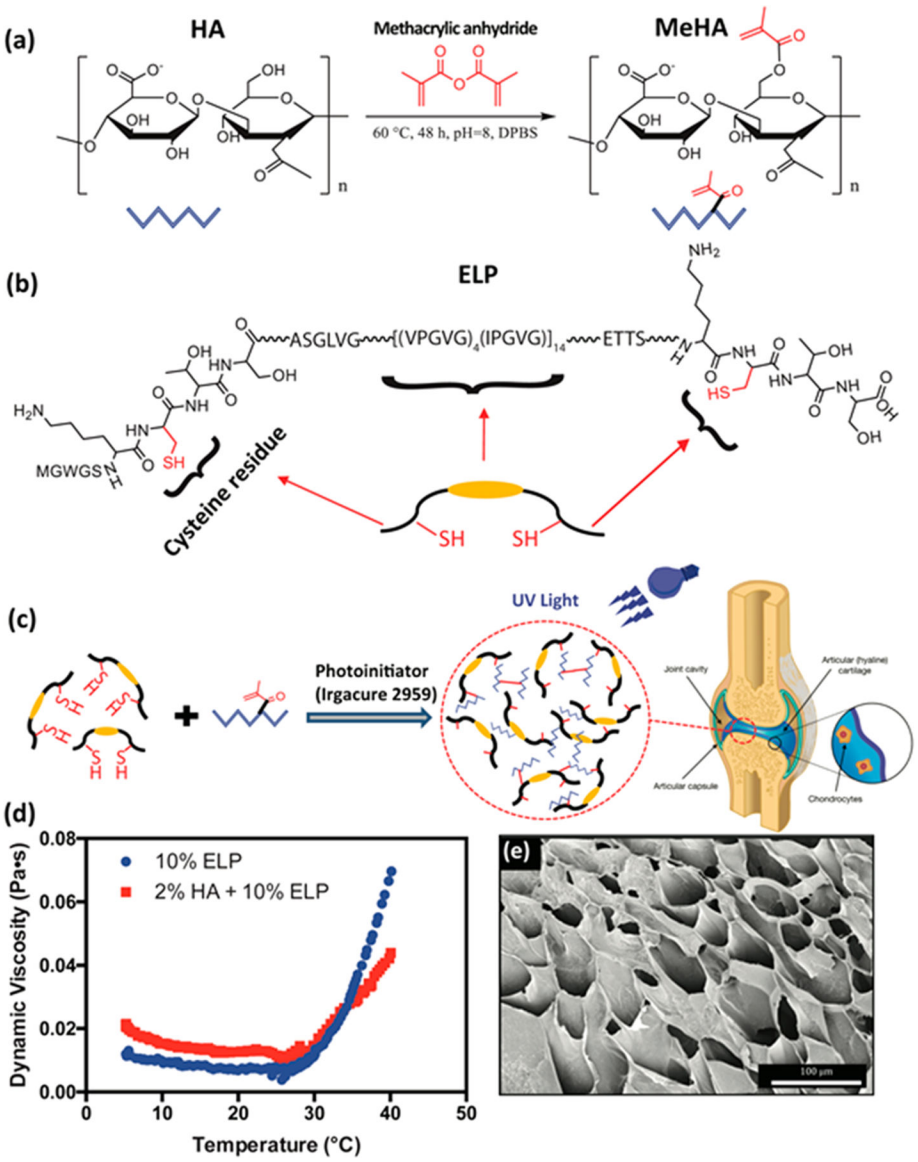

Figure 1.

Schematic of MeHA/ELP hydrogel formation and chemical structure. (a) HA methacrylation to form MeHA; (b) chemical structure of ELP, indicating the presence of cysteine residues; and (c) schematic diagrams of photo-cross-linking of MeHA/ELP hydrogels and potential application of the adhesive composite. (d) Variation in dynamic viscosity of the ELP and MeHA/ELP prepolymers by temperature, showing phase transition temperature (T_t). (e) A representative SEM image of a MeHA/ELP hydrogel synthesized by 2% MeHA and 10% ELP.

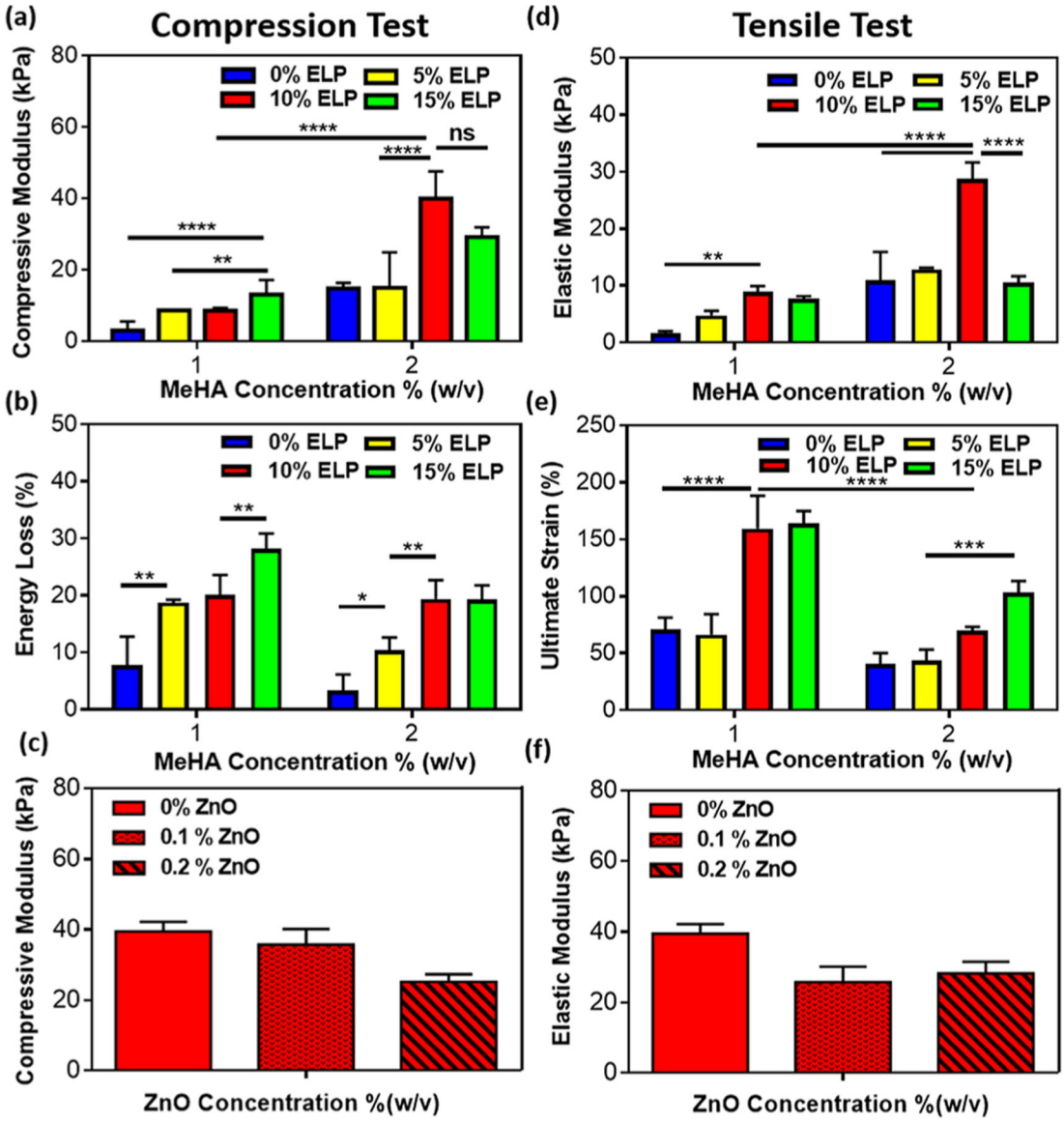

Figure 2.

Mechanical properties of photo-cross-linkable MeHA/ELP hybrid hydrogels. (a) Compressive modulus and (b) energy loss of MeHA/ELP hydrogels produced by using different MeHA and ELP concentrations. (c) Compressive modulus of MeHA/ELP hydrogels (2% MeHA and 10% ELP) containing different ZnO concentrations (0, 0.1 and 0.2%(w/v)). (d) Elastic modulus and (e) ultimate tensile strain of MeHA/ELP hydrogels produced using different MeHA and ELP concentrations. (f) Elastic modulus of MeHA/ELP hydrogels (2% MeHA and 10% ELP) containing different ZnO concentrations (0, 0.1 and 0.2%(w/v)). (* $p < 0.05$, ** $p < 0.01$, *** $p < 0.001$, **** $p < 0.0001$).

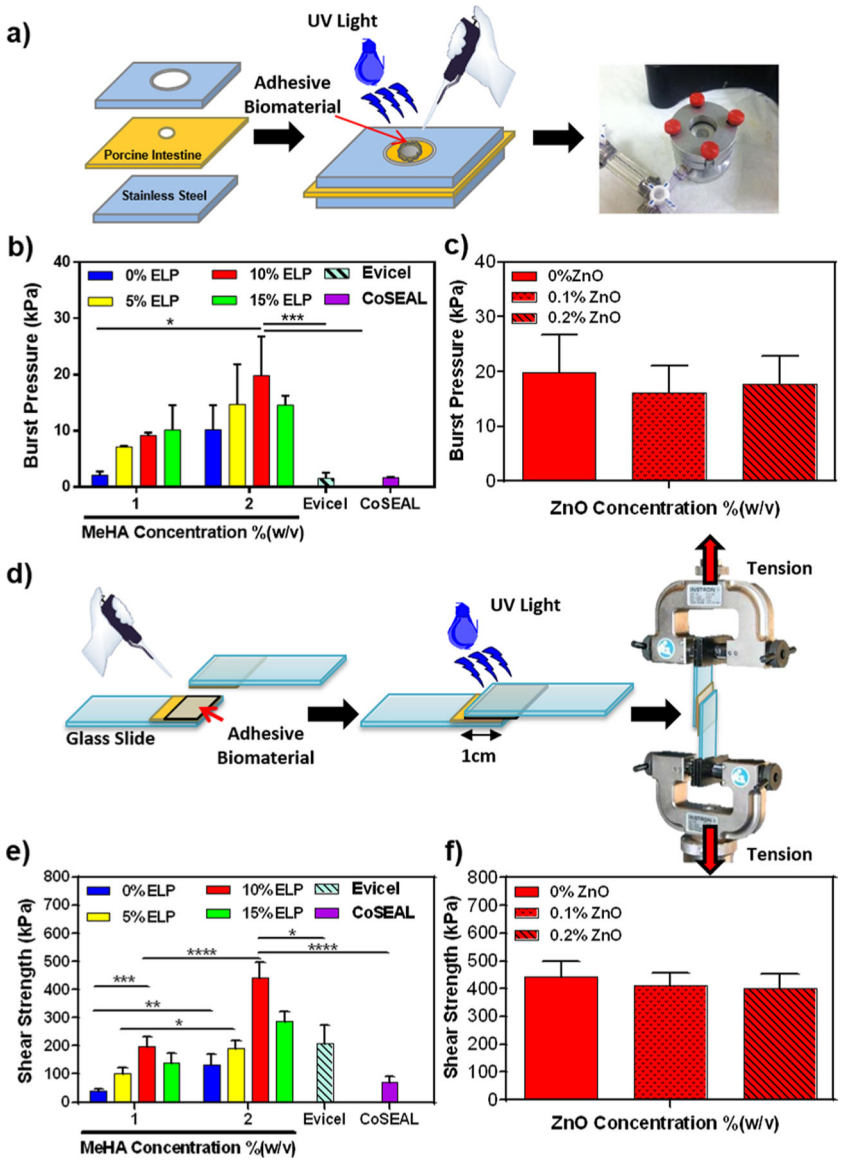

Figure 3.

Adhesive properties of photo-cross-linkable MeHA/ELP hybrid hydrogels. (a) Schematic of the modified standard burst pressure test (ASTM F2392–04). Burst pressure resistance of (b) MeHA/ELP hydrogels produced by using different MeHA and ELP concentrations and commercially available adhesives and (c) MeHA/ELP hydrogels (2% MeHA and 10% ELP) containing 0, 0.1, and 0.2% ZnO. (d) Schematic of the modified standard lap shear test (ASTM F2255–05). Shear strength of (e) MeHA/ELP hydrogels produced by using different MeHA and ELP concentrations and commercially available adhesives and (f) MeHA/ELP hydrogels (2% MeHA and 10% ELP) containing 0, 0.1, and 0.2% ZnO (* $p < 0.05$, ** $p < 0.01$, *** $p < 0.001$, **** $p < 0.0001$).

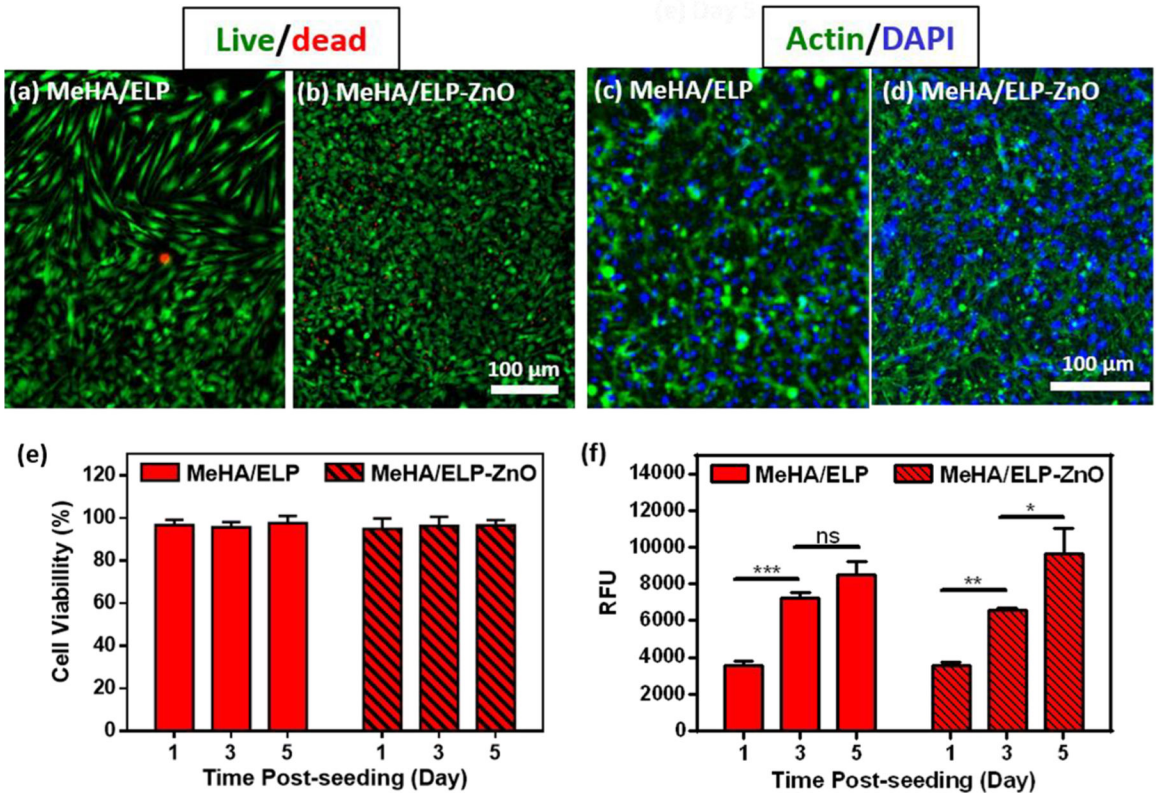

Figure 4.

In vitro cytocompatibility of MeHA/ELP and MeHA/ELP-ZnO hydrogels. Representative live/dead images from hMSCs seeded on (a) MeHA/ELP and (b) MeHA/ELP-ZnO hydrogels after 5 days of seeding. Representative phalloidin (green)/DAPI (blue) stained images from hMSCs seeded on (c) MeHA/ELP and (d) MeHA/ELP-ZnO hydrogels at day 5 post culture. Quantification of (e) viability and (f) metabolic activity of hMSCs seeded on hydrogels after 1, 3, and 5 days of culture. Hydrogels were formed by using 2% MeHA and 10% ELP with 0 and 0.2%(w/v) ZnO nanoparticles at 120 s UV exposure time (* $p < 0.05$, ** $p < 0.01$, *** $p < 0.001$).

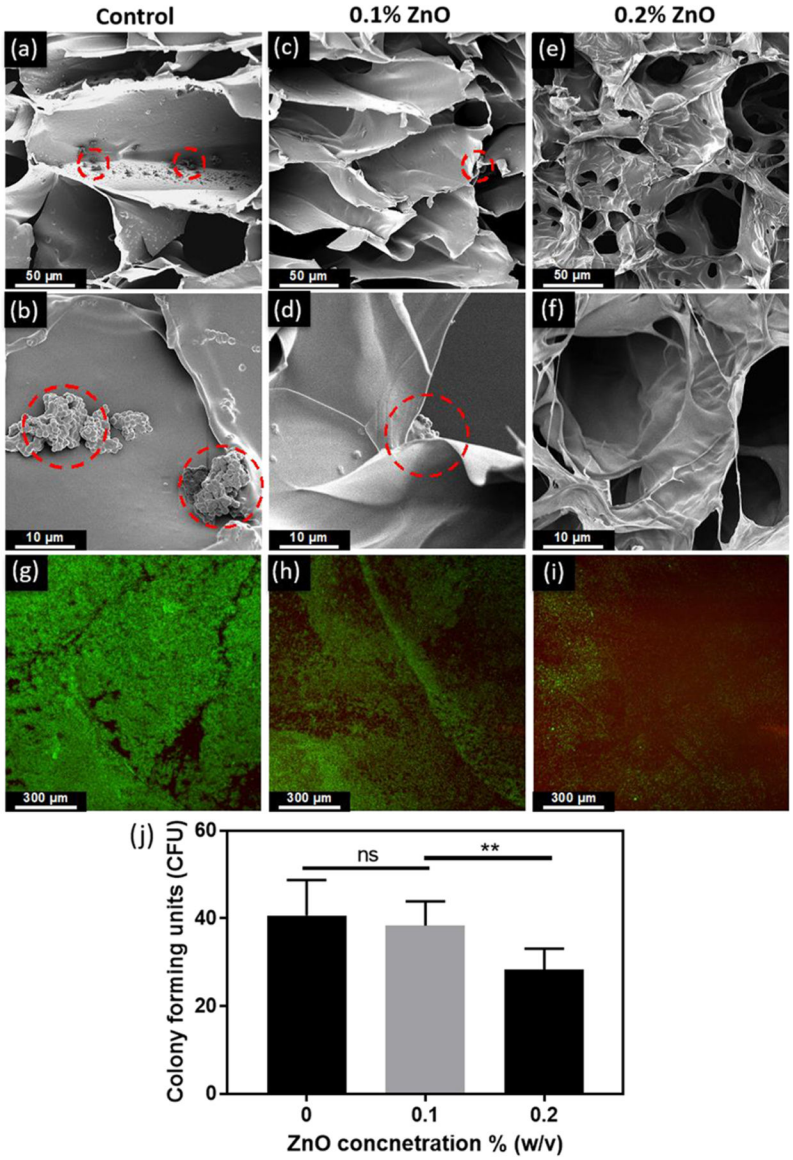

Figure 5.

In vitro antimicrobial properties of MeHA/ELP-ZnO hydrogels with different ZnO concentrations. Representative SEM images of methicillin-resistant *Staphylococcus aureus* (MRSA) colonization on hydrogels containing (a, b) 0% ZnO, (c, d) 0.1% ZnO, and (e, f) 0.2% ZnO. Clusters of bacteria are shown in dashed circles. (g) Representative live/dead images from bacteria seeded hydrogels containing (g) 0% ZnO, (h) 0.1% ZnO, and (i) 0.2% ZnO after 1 day of incubation. (i) Colony counting results of different ZnO concentrations in ZnO/HA-ELP hydrogels. Hydrogels were formed by using 2% MeHA and 10% ELP at 120 s UV exposure time (** $p < 0.01$).

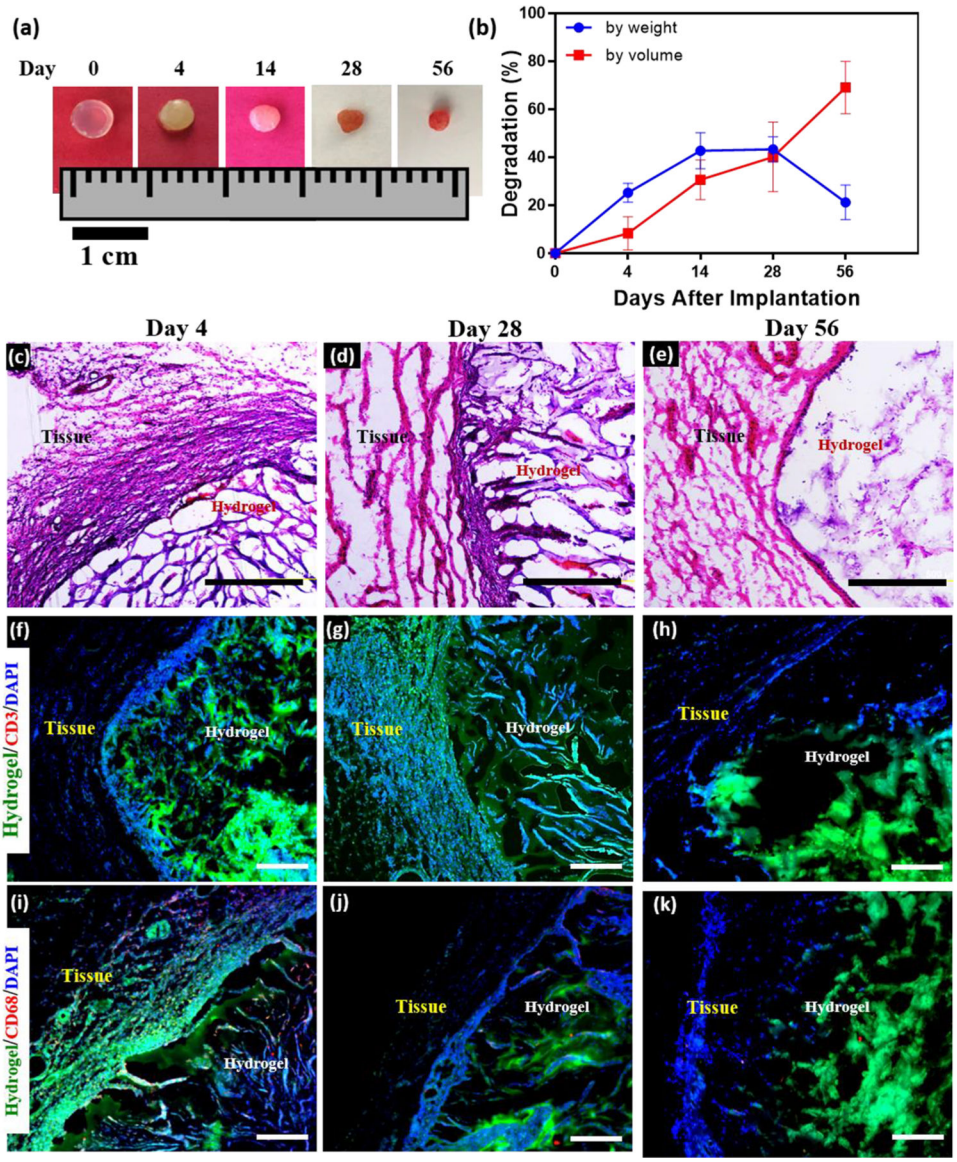

Figure 6.

In vivo biocompatibility and biodegradation of MeHA/ELP hybrid hydrogels using a rat subcutaneous implantation model. (a) Representative images of MeHA/ELP hydrogels before implantation (day 0) and on days 4, 14, 28, 56 post implantation. (b) In vivo biodegradation of MeHA/ELP hydrogels on days 0, 4, 14, 28, and 56 of implantation, based on weight and volume loss of the implants ($n = 4$). The in vivo degradation profile of MeHA/ELP hydrogels shows an approximately linear degradation behavior by volume during the first 56 days after implantation, as well as the highest biodegradation by weight between days 14 and 28. Hematoxylin and eosin (H&E) staining of MeHA/ELP sections (hydrogels with the surrounding tissue) after (c) 4, (d) 28, and (e) 56 days of implantation (scale bars = 500 μm). Immunohistofluorescent analysis of subcutaneously implanted MeHA/ELP hydrogels showing no significant local lymphocyte infiltration (CD3) at (f) 4, (g) 28, and (h) 56 days post implantation (scale bars = 200 μm). Fluorescent images

showed transient macrophage infiltration (CD68) at (i) day 4, followed by no apparent positive fluorescence at (j) 28 and (k) 56 days post implantation (scale bars = 200 μm). Green, red and blue colors in (f–k) represent the MeHA/ELP autofluorescent hydrogels, the immune cells, and cell nuclei (DAPI), respectively. Hydrogels were formed by using 2% MeHA and 10% ELP at 120 s UV exposure time.